OBSERVATIONAL STUDY OF THE FIVE-MINUTE OSCILLATIONS IN THE SOLAR ATMOSPHERE

I. *Oscillatory Velocity and Intensity Fields*

K. R. SIVARAMAN
Indian Institute of Astrophysics, Kodaikanal, India

(Received 4 May; in revised form 5 October, 1973)

Abstract. The 5-min oscillations in the photospheric velocity fields have been studied in detail from measurements on 14 absorption lines from three time sequences of spectrograms of high quality. The lines cover a range of heights in the solar atmosphere from log $\tau = +0.2$ to -1.2. Regions oscillating coherently are seen to have an average dimension of 8000 km and the oscillations in general last for 2 to 3 periods. The power spectrum analysis of high resolution enabled to determine the period of oscillation at each level very precisely. The period decreases with increase in height, being 304 s at the level log $\tau = +0.2$ and 295 s at the level log $\tau = -1.2$. The low level lines possess considerable power in the low frequency range representing the convective overshoot from below. The oscillatory power increases with height, while the low frequency power decreases and the high frequency component remains substantially constant in the heights studied.

The intensity fluctuations in the continuum, the line wing and core of Fe I 6358.695 have also been studied. The continuum power spectrum has practically all the power near the zero frequency range, with a very weak oscillatory component. The line wing intensity fluctuations resemble those in the continuum, whereas the line core clearly shows an oscillatory component similar to the velocity oscillations.

1. Introduction

The study of the dynamical characteristics of the velocity fields in the quiet regions on the Sun during the past two decades has enabled significant advancement of our knowledge in this direction. Since the discovery by Leighton *et al.* (1962) of the small scale vertical oscillations in the velocity fields in the upper photosphere and low chromosphere, Evans *et al.* (1963), Edmonds *et al.* (1965) and Frazier (1968) have studied these oscillations using time sequence spectra. The velocity oscillations have also been studied using the one-dimensional scans obtained with a magnetograph in the Doppler mode by Howard (1968), Deubner (1967, 1972), Tanenbaum *et al.* (1969), Musman and Rust (1970) and Bhattacharyya (1972). Considerable data have accumulated throughout the years by many investigators using one technique or the other, most of them oriented towards studies of the temporal properties of the velocity oscillations, with observations on 2 or 3 spectral lines at one time. It would be desirable to know the depth dependent properties of these oscillations combined with the time parameter. The present investigation is an analysis with time sequence spectra covering a number of lines to study their depth-wise properties.

2. The Observations

The observations were made with the horizontal solar tower telescope and the 18-m spectrograph at the Kodaikanal Observatory. A two-mirror fused quartz coelostat

Solar Physics **33** (1973) 319–331.

of 61 cm aperture feeds a 38 cm two-element achromat of 36 m focal length. The image scale of the telescope is 5.5″ per mm. The Littrow spectrograph has a 20 cm two-element achromat of 18.3 m focal length and a Babcock grating of ruled area 135 × 200 mm with 600 grooves mm^{-1} and blazed in the fifth order green. A number of time sequences of spectra were obtained around chosen spectral regions with the spectrograph slit located on quiet regions near the centre of the solar disc. The effective length of the slit was 19 mm and a width of 100 μ was maintained in all the sequences. A hair stretched across the spectrograph slit during the observations served as a fiducial line along the direction of dispersion. The overlapping orders of the grating were eliminated with wide-band glass colour filters. The solar rotation was compensated in proper amounts so that the same part of the Sun lay over the slit throughout the period of observation. The spectra were obtained within two hours after sun-rise, when the visibility at Kodaikanal is usually at its best. The exposure time was continually decreased to compensate for the increase in brightness of the solar image due to the rapid change in the value of s z. 35 mm film in spools of 100 ft were used in a camera with mechanical film transport. The films were calibrated with a six-step wedge and an out of focus image of the centre of the solar disc.

Of the many sequences, three sequences obtained under exceedingly good visibility conditions were chosen for the present study. The details of the spectra are given in Table I.

TABLE I

Details of the time sequences

Sequence designation	Date	Spectral region	Grating order	Dispersion	Emulsion	Time between exposures	Duration of the sequence
A 1082	Apr. 16, 1969	6340 Å	IV	6.677 mm $Å^{-1}$	Kodak IV-E	20″	40′
A 1100	Jan. 11, 1970	6587 Å	IV	7.096 mm $Å^{-1}$	Kodak IV-E	20″	22′
A 1133	Mar. 12, 1971	4280 Å	VI	10.306 mm $Å^{-1}$	Ansco Hypan-X	15″	40′

The high image quality shown by the high contrast in the continuum streaks and the line wiggles are maintained throughout the lengths of the sequences without significant change. The full-width at half maximum (FWHM) of the auto-correlation curve of the granulation intensity field was 1100 km which may be considered as an average value, while the best isolated frames have a FWHM of 800 km. The average value of our sequence is identical with that of the time sequence obtained under excellent visibility conditions by Evans at Sacramento Peak and studied by Edmonds *et al.* (1965). The guiding excursions could not have exceeded ±0.5″; this accuracy being ensured by the photoelectric guiding employed in the observations. This is also confirmed by the correlation coefficient of the continuum fluctuations of successive frames which has a value of 0.99 from the beginning to the end of the sequences.

3. Measurements

Fourteen spectral lines were chosen for the study from the three sequences. Details of these lines are shown in Table II.

Sequence A 1100 includes 6587.622 Å of atomic carbon formed in the very deep photospheric layers. The eight lines in A 1082, include a Si II line, of high excitation potential. These two sequences were obtained on Kodak IV-E emulsion which combines high contrast and low granularity, quite suited to measure small Doppler shifts in these hazy deep lying lines. The noise level in these lines is, however, not negligible compared to the other lines studied. The fourteen lines have their mean depths of formation well distributed in height in the solar atmosphere, ranging almost from the granulation layers through the photosphere up to the low chromosphere. The contribution curves of 8 lines were computed using the Elste model atmosphere (Elste, 1967) by the 'weighting function' method taking into account the saturation function of Pecker.

The Doppler displacements in the spectral lines were measured with a Doppler comparator of the Kodaikanal Observatory (Kubicela and Sivaraman, 1969). The location of the two slits of the comparator on the line profile $\pm\Delta\lambda$, at which the Doppler shifts were measured and the width of the slits used 'W' in Å are included in Table II. The slits were located on the steepest part of the profile to provide the highest

TABLE II

Details of the spectral lines included in this study

Sequence designation	Line	Element	Rowland intensity	Excitation potential lower level	$\pm\Delta\lambda$(Å)	W(Å)	ξ km s^{-1}
A 1082	6330.859	Fe I	2	4.73	0.0464	0.0329	0.31
	6335.345	Fe I	6	2.188	0.0659	0.0419	0.34
	6336.837	Fe I	7	3.67	0.0659	0.0419	0.35
	6338.588	Fe I	2	4.79	0.0464	0.0329	0.32
	6339.125	Ni I	2	4.136	0.0464	0.0329	0.31
	6344.162	Fe I	4	2.422	0.0584	0.0329	0.34
	6347.104	Si II	2	8.085	0.0479	0.0928	–
	6358.695	Fe I	6	0.855	0.0659	0.0419	0.39
	6342.389	Telluric		–	0.0374	0.0329	–
A 1100	6572.795	Ca I	1	0.000	0.0437	0.0310	0.30
	6586.319	Ni I	1	1.942	0.0437	0.0395	0.30
	6587.622	C I	−1	8.53	0.0613	0.0592	0.34[a]
	6593.884	Fe I	4	2.43	0.0437	0.0395	0.30
	6586.511	Telluric		–	0.0352	0.0310	–
A 1133	4281.974	CH	2	–	0.0427	0.0272	0.34
	4283.016	Ca I	4	1.878	0.0427	0.0272	0.35

$\xi = \sqrt{2}$ times rms velocity.

[a] Velocity records are noisy and hence have a high value of ξ.

accuracy and their widths were kept as low as possible to avoid considerable depth averaging in the solar atmosphere. The two sources of noise in the measurements are due to the plate grain and turbulence inside the spectrograph. The grain noise for the Ansco Hypan-X estimated from measurements was found to be 40 m s^{-1}. The rms value of the turbulence computed from measurements of the shifts on the telluric lines in sequences A 1082 and A1100 is 59 m s^{-1}.

4. Analysis

4.1. Practical procedure

Measurements at the comparator yielded a $A(X_i)$ curve of velocity for each spectral line at 61 points along the slit of the spectrograph, regularly spaced 1080 km apart. The A 1082 sequence has 120 frames exposed successively. The velocity data consist of a two dimensional array $A(X_i, t_j)$ with i running from 1 to 61 and j running from 1 to 120. For sequence A 1100, with 62 exposures, the array has 62 columns and 61 rows. Sequence A 1133 has an array of 160 columns and 61 rows. The $A(X)$ curves of successive frames of one line in each sequence when plotted and superposed, matched very well everywhere and did not show any sign of the declination drift along the slit within detectable limits. The $A(X)$ curves for the two telluric lines one each from A 1082 and A 1100 measured as for the solar lines represent the turbulence in the Earth's atmosphere and inside the spectrograph. These were averaged to give two mean $A(X)$ curves. The mean curve which has a shape that results from the curvature of spectral lines due to reflection from a plane grating formed the reference curve. For the sequence A 1133 the reference curve was derived by averaging the 160 velocity curves of one of the solar lines. The reference curve was fitted to each $A(X)$ curve at its mean value and the deviations were read out at the 61 points. This method of obtaining velocities with respect to the mean over each frame automatically filters out all modes of large horizontal wavelengths, particularly those of the supergranulation cells. The very small wavelengths are also filtered by choosing the 1080 km steps.

The deviations $V(X_i, t_j)$, forming the fluctuating component of the velocity, were converted to vertical velocities in km s^{-1}, using the Doppler relation. These were done on a CDC 3600 computer. The output of the computer consists of data points forming a $V(X_i, t_j)$ array and reading horizontally, a $V(t)$ curve can be obtained. Sample plots of such $V(t)$ curves for two spectral lines are shown in Figure 1.

The oscillations with measurable amplitudes occupy a substantial part of the solar surface. The regions oscillating coherently have dimensions of 10–12″ along the slit or an average extent of 8000 km on the Sun. The rms of the amplitude determined from the prominent oscillations is given in Table III. These do not show a definite increase, although there is a suggestion of this. Individual bursts of oscillations with amplitudes of 200 m s^{-1} and above last in general for 10 to 15 min. The occurrence of oscillations in bursts have prompted many workers to favour the model, where the granules act as individual pistons giving rise to oscillatory motions. This appears a simplification of the real situation. Such individual impulses generated in a random

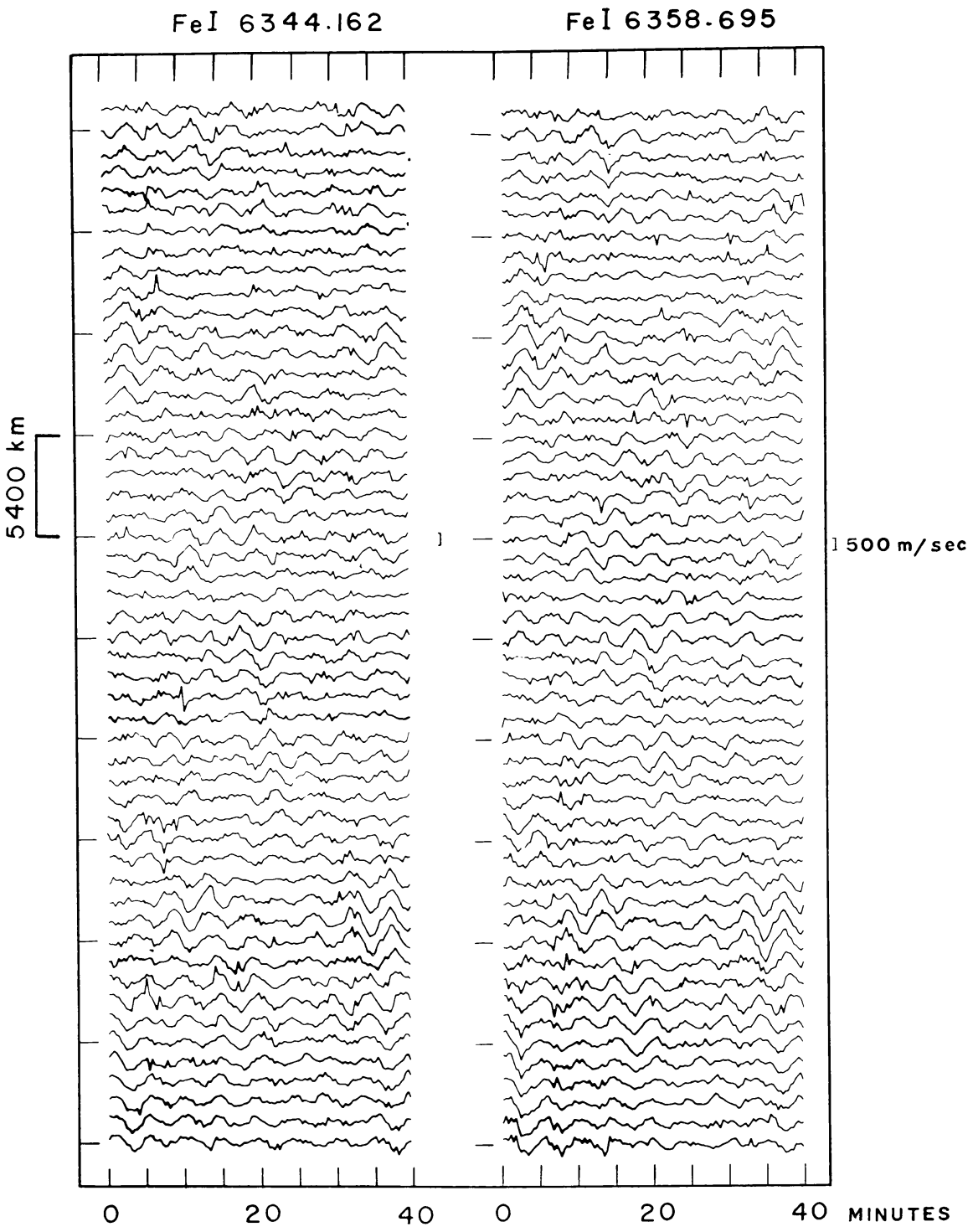

Fig. 1. Sample plot of velocity vs time and position. The curves represent the velocity at consecutive points, separated by 1080 km on the Sun.

TABLE III

Characteristics of the oscillations

Line λ(Å)	Mean depth of formation log τ	Period (s)	Rms amplitude km s^{-1}.
Fe I 6358.695	−1.2	295	0.28
Fe I 6344.162	−1.0	295	0.26
Fe I 6335.345	−1.0	295	0.28
Fe I 6593.884	–	295	0.23
Ca I 6572.795	−1.0	295	0.24
Fe I 6336.837	−0.8	295	0.23
Ni I 6586.319	–	295	0.23
Ni I 6339.125	–	295	0.22
CH 4281.794	−0.8	295	0.23
Ca I 4283.016	−0.6	295–300	0.25
Fe I 6338.588	−0.6	295–300	0.22
Fe I 6330.859	–	295–300	0.22
C I 6587.622	+0.2	304	0.41 [a]

[a] Value high as the records are noisy.

manner by the granular pistons cannot maintain the oscillations coherently over a scale many times the size of the granules themselves.

The two lines 6330.859 Å and 6338.588 Å are of the same intensity and excitation potential values. In spite of this, their velocity plots have only as much resemblance as with any other lines studied; the similarities do not extend up to the smallest features.

4.2. Power spectrum analysis

The power spectra for all the lines were computed from the Fourier transform of the autocorrelation functions of the velocity data, by the methods described by Blackman and Tukey (1958). For each line, we obtained the power spectra for the 61 points along the slit and also the power spectrum averaged over the 61 points. Sample plots of the power spectrum of individual points on the slit for four lines are shown in Figure 2. The regions oscillating coherently can be picked out easier by their high power. The frequency (or period) shift in the curves can be noticed. Occasionally there are curves with double peaks, and while the curves above and below – within the coherence length of 10–12″ – show no distinct double peaks, they do possess periods coinciding with one or the other of the double peaks. The peaks are at 337″ and 236″. It is possible that Frazier's study (1968), which covered 10″ × 10″ area on the Sun, was located on such a region. It can also be seen that Fe I 6335.345 shows multiple peaks at the slit positions 42, 43, 44 and 45. Similar multiple peaks are present in the plots of the lines Fe I 6336.837 and Ni I 6339.125. The latter plots are not shown here. Multiple peaks are not so evident in the same positions for the other lines, but there are suggestions of subsidiary peaks around the main peak. This indicates that these

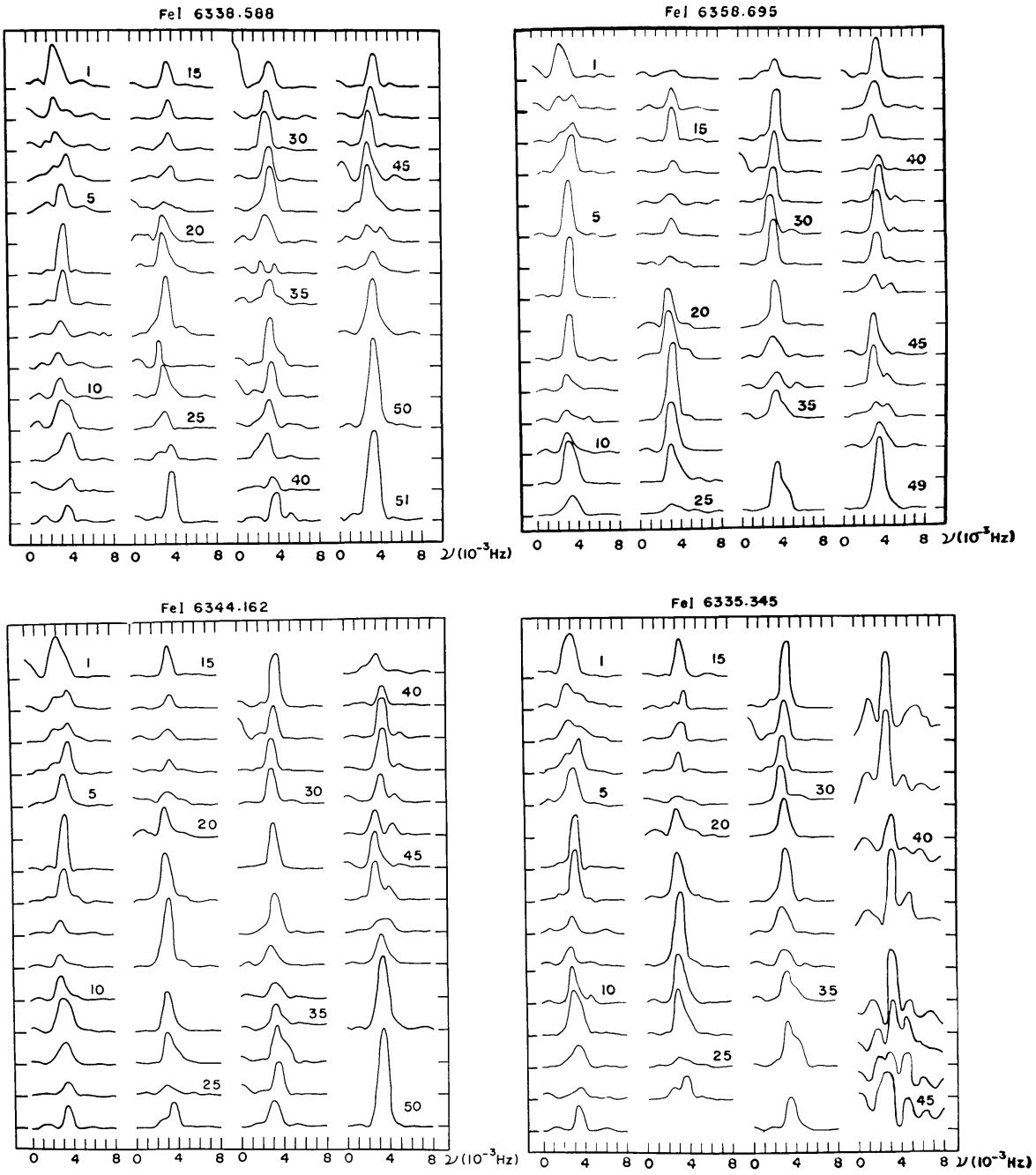

Fig. 2. Power spectra of velocities in four lines. The consecutive numbers indicate the location of the points along the slit where velocities were measured. The vertical scales represent the power.

peaks are not of statistical origin depending on the method of analysis, but are present in the solar atmosphere at certain levels, possibly representing extreme examples of local inhomogeneities. The average power spectra for all the lines are shown in Figure 3. They show pronounced peak power around 300 s which represents the resonance period of the oscillations in the solar atmosphere. The spectrograms of A 1082, obtained at high resolution, showed Si II 6347.104 to be a very close doublet having components of nearly the same strength. The Utrecht Atlas shows this line to have un-

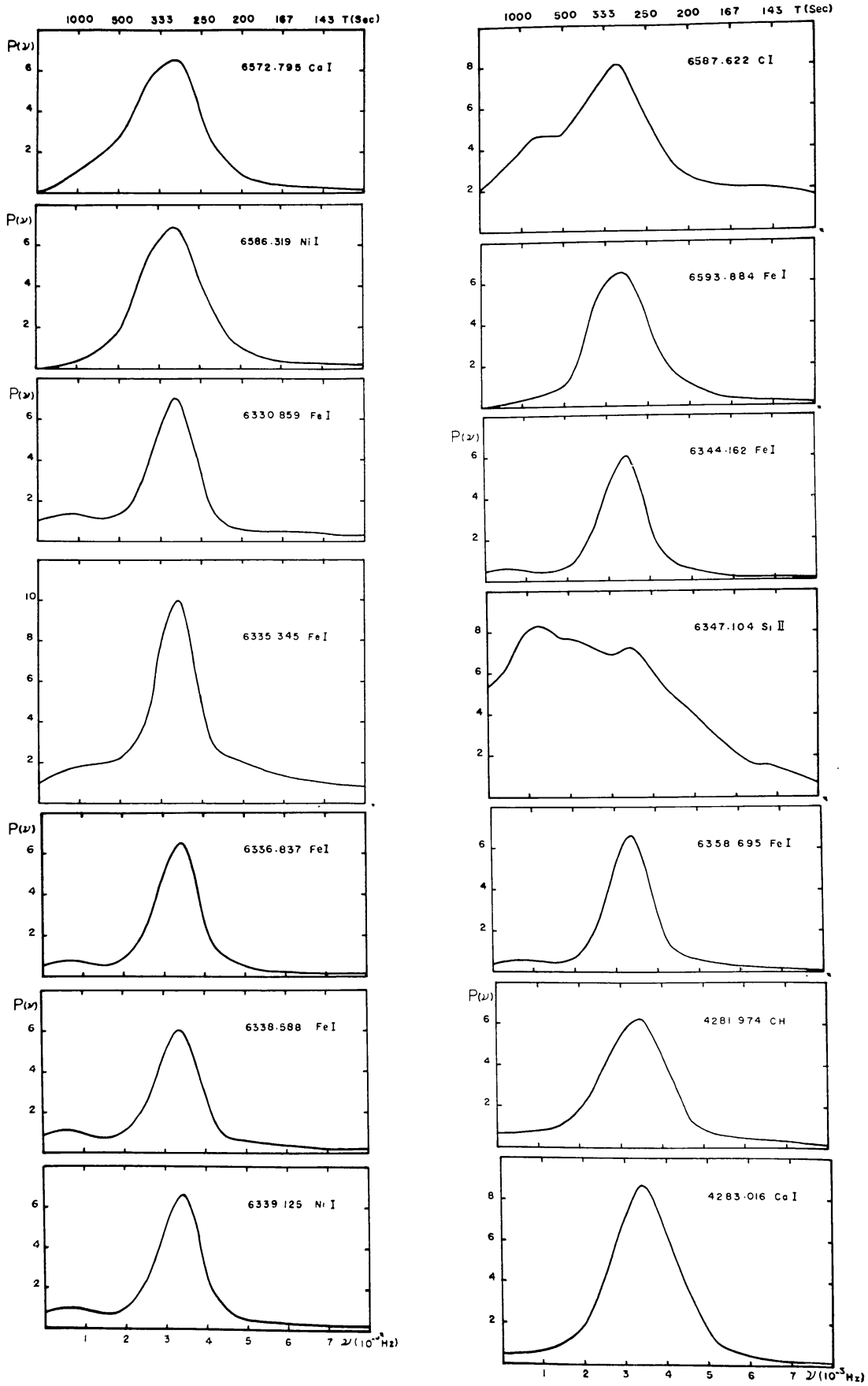

Fig. 3. Average power spectra of the velocities in the spectral lines.

doubtedly clean wings. In the measurement of Doppler shifts, one slit of the comparator was located on the violet wing of one line and the other slit on the red wing of the other line. While the power spectrum resembles that due to random noise, it still shows peaks around $\nu = 1.25 \times 10^{-3}$ Hz and $\nu = 3.33 \times 10^{-3}$ Hz, characteristic of a low level line.

4.3. Power spectrum analysis of high resolution

The power spectra above were obtained by the usual method wherein one value for maximum lag is used in the calculation of the A.C. functions, this value of the lag being chosen to yield estimates in the neighbourhood of frequencies, where the suspected periodicities lie. But, with limited length of data, the power spectrum obtained has usually a poor frequency resolution for the spectral estimates. In the present analysis we have computed the estimates for five different lags, with values chosen close to one another and around 30% of the total length of the data. With the estimates

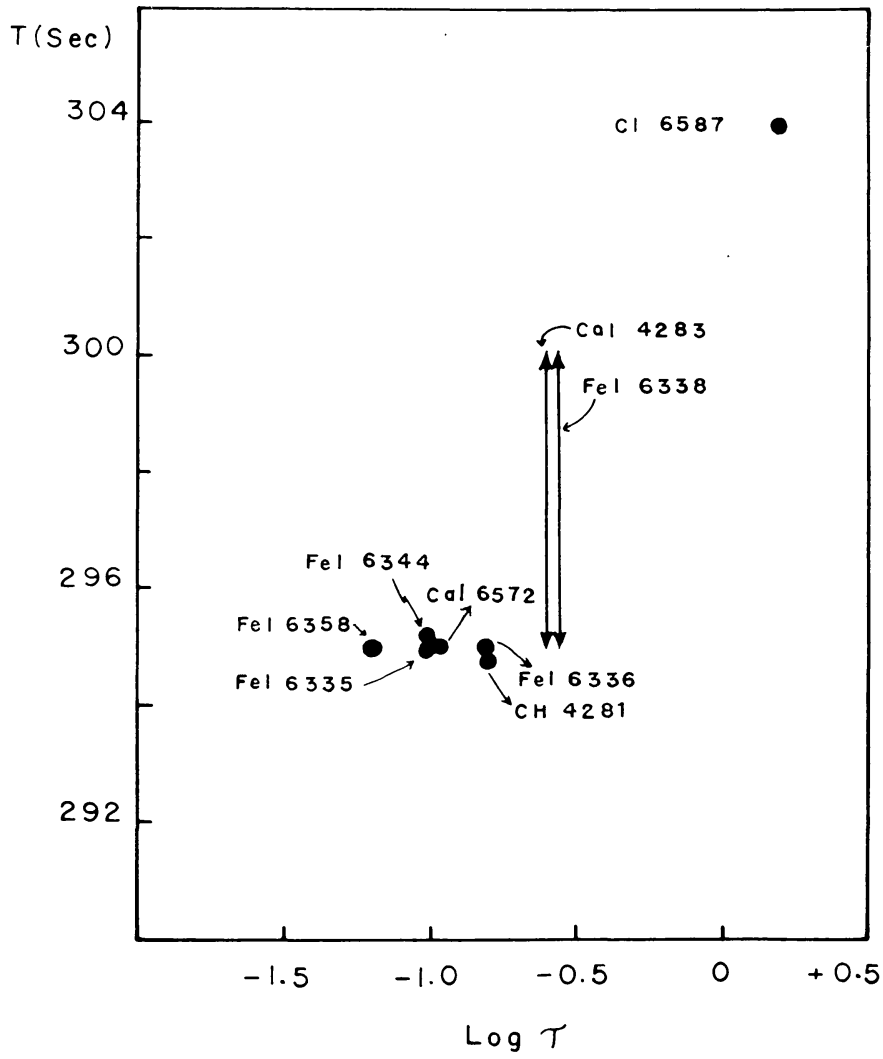

Fig. 4. Relation between the period of oscillation observed in the lines against their mean depth of formation in terms of log τ.

for the different lags put together the frequency resolution can be considerably increased. For sequence A 1082, the power spectrum with 29 lags gives estimates at 286.6″, 232″; with 30 lags the estimates are at 400″, 300″, and 240″, besides at other periods. Similarly lags 31, 37, 38 give estimates at periods 310″, 296″, 304″, respectively, besides for periods below and above these. The power spectral density derived from all the five lags for the periods 290, 296, 300, 304 and 310″, can then be compared after applying a correction. The bandwidth corresponding to each estimate may be taken as $1/T_m$, where T_m is the maximum value of the lag used. There is a fall in power when the lag is increased due to a decrease in bandwidth. This fall in power, can be compensated for by multiplying the spectral estimates by a factor equal to the ratio of the bandwidths. It is important that the lags lie close together to avoid a significant change in the stability of the estimates for the various lags. The value of the periods so derived for the lines are shown in Table III. Figure 4 shows a plot of the periods against the mean depth of formation of the lines.

TABLE IV

Distribution of power in the ν domain

Line λ(Å)	Total power	% power contained in oscillatory range $\nu = 2.75$–4.25×10^{-3} Hz	% power contained in low frequency range $\nu = 0$ to 1.5×10^{-3} Hz	% power contained in high frequency range $\nu = 5.5$–8.0×10^{-3} Hz	Log τ
6358.695	2125	66.1	5.1	3.7	−1.2
6344.162	2033	65.9	5.8	3.6	−1.0
6335.345	4606	61.0	10.3	12.1	−1.0
6593.884	2392	65.3	5.9	5.6	–
6572.795	3111	51.1	7.4	4.8	−1.0
6336.837	2136	63.9	9.1	3.6	−0.8
6586.319	2920	58.1	6.2	4.7	–
6339.125	2320	60.4	8.7	6.3	–
4281.794	2792	51.7	8.0	6.6	−0.8
4283.016	3869	55.8	5.0	3.8	−0.6
6338.588	2260	57.9	12.1	6.0	−0.6
6330.859	2749	55.3	11.9	7.7	–
6587.622	6461	35.1	15.9	15.5	+0.2

Table IV shows the relative content of percentage of power in the low, oscillatory, and high frequency ranges for all the lines. These were obtained from the areas of the curves of Figure 3. The total power is directly the area in square units. The lines are arranged according to their mean depth of formation. It is seen that the oscillatory range gains in strength with increase in height in the solar atmosphere and the low level lines possess significant power in the low frequency range. A minor peak at $\nu = 1.25 \times$ $\times 10^{-3}$ can also be seen in the C I 6587 line. This low frequency power decreases fast with height, in agreement with the findings of Edmonds *et al.* (1965). The high frequency tail remains substantially constant in the range of heights studied.

4.4. Intensity fluctuations

To study the intensity fluctuations in the continuum, the line wings, and core of Fe I 6358.695 of the A 1082 sequence, measurements were made on 62 frames out of the 120 frames of the sequence from the microdensitometer traces. The continuum is exposed to a degree that is favourable for studying the brightness fluctuations. For the line wing intensities, the microphotometer slits were located practically at the same $\pm\Delta\lambda$ value as in the velocity measurements, but the dimensions of the slits being smaller, the depth averaging is less in the intensity measures. The effect of the Doppler shifts were eliminated by averaging the traces at $+\Delta\lambda$ and $-\Delta\lambda$. The density points read at intervals of 1080 km on the Sun were converted into intensities via the calibration curve. The fiducial line for stepping off this interval for the density points was again the shadow of the hair line on the spectrograph slit. This ensured that the intensities read off, and the earlier velocity measurements pertain to the same region on the Sun. The mean line derived by averaging the intensity measures of 62 frames was fitted to each $I(X)$ curve and the deviations $\Delta I(X)$ were read off at the 61 points

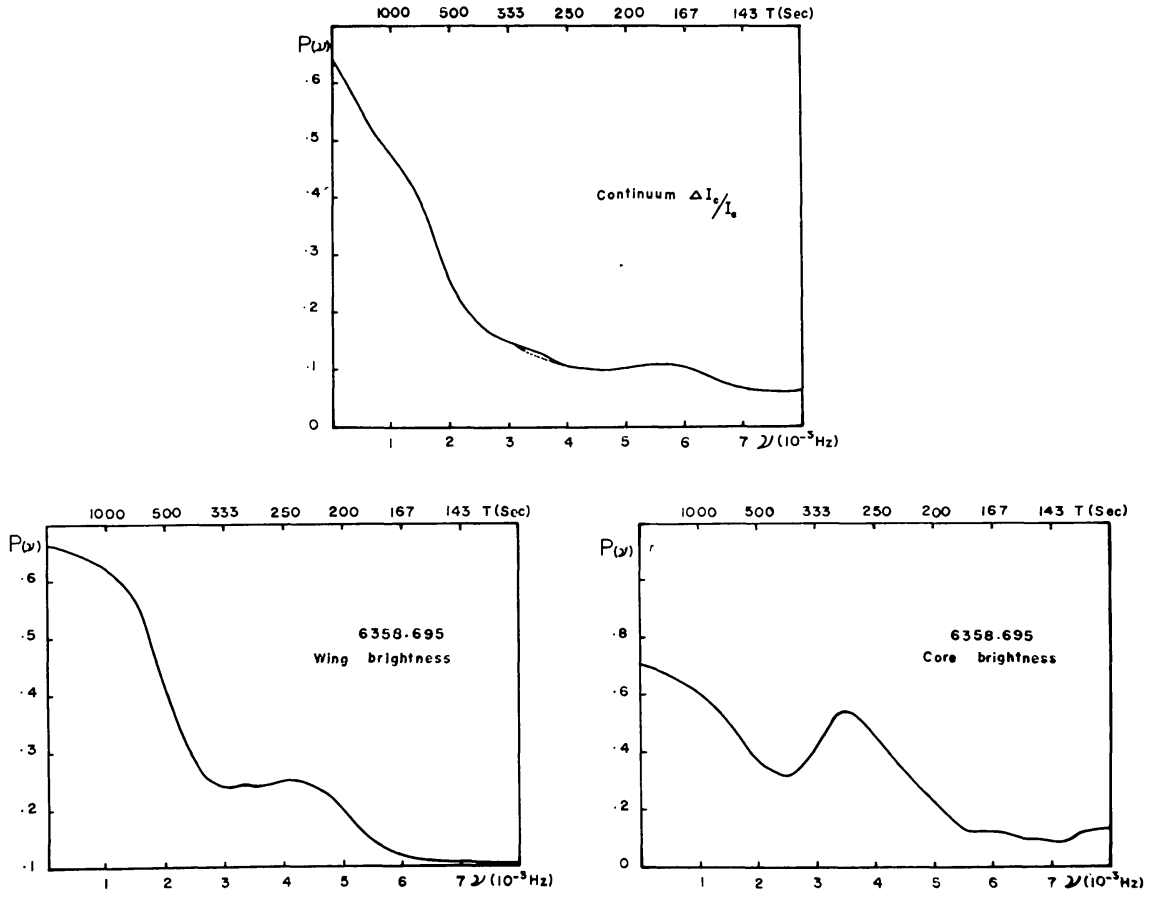

Fig. 5. Power spectra of the intensity fluctuations; (a) in the continuum, (b) in the wing of Fe I 6358.695, (c) in the core of Fe I 6358.695. The peak at $\nu = 3.5 \times 10^{-3}$ Hz is prominent, showing the presence of the oscillatory component.

along the slit. With these, values of

$$\frac{\Delta I_{\text{cont}}}{I_{\text{cont}}}, \quad \frac{\Delta I_{\text{Wing}}}{I_{\text{Wing}}} \quad \text{and} \quad \frac{\Delta I_{\text{core}}}{I_{\text{core}}}$$

were computed. The time power spectra of these obtained as with velocities are shown in Figure 5.

5. Discussion of Results

The observations described above show the solar surface to be covered with oscillations, but a careful scrutiny will reveal that these oscillations are complex in nature. There are regions in between the prominently oscillating areas, where the oscillations are hardly detectable. Even in the prominent oscillations, the wave-pattern is that of a heavily distorted sine wave. It may be that the slowly varying component due to the convective motions, which is known to exist along with the oscillatory motions, damp these oscillations. Interference with the oscillations of neighbouring cells can be another contributing factor. This latter effect can be studied by observing oscillations at two or three locations near the centre of the disc and separated by about thrice the dimensions of the oscillating cells.

Our analysis of high resolution clearly shows a decrease in period with height increase. In an isothermal atmosphere, the propagation is characterised by two critical frequencies ω_1 and ω_2; frequencies greater than ω_1 representing sound waves propagating vertically upwards and those less than ω_2 representing gravity waves. If we accept the argument of Moore and Spiegel (1964) that the observed oscillations are forced oscillations excited by the non-propagating frequencies in the interval $\omega_1 - \omega_2$, then at any height only frequencies $> \omega_1$ can propagate upwards without attenuation. The other alternative, namely the gravity waves, cannot exist at these levels due to the low radiative cooling time (Souffrin, 1966). Thus the solar atmosphere acts as a high-pass filter, filtering out all frequencies less than ω_1, the value of ω_1 itself increasing monotonically with height due to change in the physical conditions. Thus, in the frequency spectrum, the frequency possessing maximum power shifts towards high frequencies with height.

The continuum intensity power spectrum starts with maximum power at zero frequency, falling off rapidly at higher frequencies, typical of convective motion. It shows a very weak oscillatory component at $\nu = 3.5 \times 10^{-3}$ Hz. The line wing variations resemble very well those of the continuum. The line core brightness fluctuations has two regions of maximum power, one near the zero frequency and another at $\nu = 3.5 \times 10^{-3}$ Hz, which is the resonance range corresponding to the velocity field.

In the low frequency range, the low level lines possess considerable power, both in the velocity and intensity power spectra. This appears to be due to the convective component of the macroscopic velocity field in the low photosphere. In the case of the intensity power spectra, part of this low frequency power could arise from the persistent structures as interpreted by Evans *et al.* (1963). This is in conformity with the prediction of the 'convective overshoot' into the stable layers of the photosphere.

The observations of Bray and Loughhead (1967) also show that the granules are visible up to an optical depth of $\tau = 0.1$. The other possibility for this low frequency component is the existence of gravity waves from frequency considerations alone; but these cannot, however, sustain at these levels. The high-frequency component seen in all the lines possibly represent the sound waves travelling up, providing the energy for the heating of the upper chromosphere and the corona.

References

Bhattacharyya, J. C.: 1972, *Solar Phys.* **24**, 274.
Blackman, R. B. and Tukey, J. W.: 1958, *The Measurement of Power Spectra*, Dover Publications, N.Y.
Bray, R. J. and Loughhead, R. E.: 1967, *The Solar Granulation*, Chapman and Hall Ltd., p. 32.
Deubner, F. L.: 1967, *Solar Phys.* **2**, 133.
Deubner, F. L.: 1972, *Solar Phys.* **22**, 263.
Edmonds, Jr., F. N., Michard, R., and Servajean, R.: 1965, *Ann. Astrophys.* **28**, 532.
Elste, C.: 1967, in C. de Jager (ed.), *The Structure of the Quiet Photosphere and the Low Chromosphere*, Proc. of the 'Bilderberg' Conference, Springer Verlag, Holland.
Evans, J. W., Michard, R., and Servajean, R.: 1963, *Ann. Astrophys.* **26**, 368.
Frazier, E. N.: 1968, *Astrophys. J.* **152**, 557.
Howard, R.: 1962, *Astrophys. J.* **136**, 211.
Howard, R.: 1967, *Solar Phys.* **2**, 3.
Kubicela, A. and Sivaraman, K. R.: 1969, *Kodai. Obs. Bull.*, Series A, No. 189.
Leighton, R. B., Noyes, R. W., and Simon, C. W.: 1962, *Astrophys. J.* **135**, 472.
Moore, D. W. and Spiegel, E. A.: 1964, *Astrophys. J.* **139**, 48.
Musman, S. and Rust, D. M.: 1970, *Solar Phys.* **13**, 261.
Noyes, R. W. and Leighton, R. B.: 1963, *Astrophys. J.* **138**, 631.
Souffrin, P.: 1966, *Ann. Astrophys.* **29**, 55.
Tanenbaum, A. S., Wilcox, J. M., Frazier, E. N., and Howard, R.: 1969, *Solar Phys.* **9**, 328.